Journal of NeuroEngineering and Rehabilitation

RESEARCH

Open Access

# Precision neuroregulation combining liquid metal and magnetic stimulation

Yuheng Wang[1,3], Junjie Lin[1,3], Kai Zhu[1,3], Yuhui Nie[1,3], Mengyuan Wang[1,3], Xiaoxu Ma[1,3], Xu Liu[1,3], Ruru Wang[1,3], Wenshu Mai[1,3], Fangxuan Chu[1,3], Ruixu Liu[1,3], Jiankang Wu[1,2,3,4], Jingna Jin[1,2,3,4], Xiaoqing Zhou[1,2,3,4], Ren Ma[1,2,3,4], Xin Wang[1,2,3,4], Tao Yin[1,2,3,4*], Zhipeng Liu[1,2,3,4*] and Shunqi Zhang[1,2,3,4*]

## Abstract

**Background** Electromagnetic field-based neuroregulation technology is a crucial technique for treating central nervous system and peripheral nervous system disorders. However, the use of invasive electrodes has unavoidable problems such as the risk of inflammation due to high hardness, electrical connections and the need for batteries. On the other hand, non-invasive magnetic stimulation has limitations such as centimeter-level focal areas and shallow stimulation depth.

**Methods** To enhance the precision and effectiveness of wireless magnetic stimulation, we employed a figure-8 magnetic stimulation coil (8-coil) to generate a magnetic field, combined with an injectable, highly conductive, and flexible liquid metal (LM) to produce a millimeter-scale focused electric field. A coaxial electric field measurement electrode was used to establish an agar phantom-based electric field measurement platform. The sciatic nerve of C57 mice was stimulated under acute anesthesia conditions, and electromyography (EMG) signals were collected to evaluate the enhancement of stimulation effects. Long-term safety was assessed through four weeks of implantation.

**Results** Theoretical analysis and finite element simulations demonstrated that the combination of LM and the 8-coil generated a millimeter-scale enhanced vector electric field within the tissue. Measured electric field distributions closely aligned with theoretical and simulation results. In the sciatic nerve experiments on mice, 1 μL of LM under a 0.45 T magnetic field significantly increased EMG signals and leg movement amplitude by approximately 500%. Long-term implantation under magnetic stimulation revealed no adverse effects.

**Conclusions** This method utilizes focused electric fields to improve the precision and effectiveness of neuromagnetic stimulation. It holds promise as a novel approach for precise stimulation. Preliminary evidence was provided for the safety of in vivo LM implantation under external magnetic fields.

*Correspondence:
Tao Yin
bme500@163.com
Zhipeng Liu
lzpeng67@163.com
Shunqi Zhang
zhangshunqi2004@126.com

[1]Institute of Biomedical Engineering, Chinese Academy of Medical Science & Peking Union Medical College, Tianjin 300192, China
[2]State Key Laboratory of Advanced Medical Materials and Devices, Tianjin 300192, China
[3]Tianjin Key Laboratory of Neuroregulation and Neurorepair, Tianjin 300192, China
[4]Tianjin Institutes of Health Science, Tianjin 301600, China

## Introduction

Electromagnetic field-based neuroregulation technology is primarily used to regulate the function of the central or peripheral nervous systems. It encompasses various methods, including deep brain stimulation, spinal cord stimulation, and transcranial magnetic stimulation [1–3]. These methods have found extensive applications in the treatment and research of various diseases, such as epilepsy, depression, post stroke movement disorders, spinal cord injuries, chronic pain [4–10]. Precise neuroregulation methods based on related technologies serve as essential therapeutic approaches and research tools in both clinical treatments and cutting-edge studies in neuroscience.

The basic principle of electromagnetic field-based neuroregulation is to directly apply current to tissues through electrodes or to generate electric fields within tissues using pulsed magnetic fields. When the electric field within the tissue exceeds the excitation threshold of the neurons, it changes the membrane permeability of the neuronal cell membrane to ions, resulting in neuronal excitation or inhibition. This approach aims to treat diseases or promote recovery [11]. Transcutaneous electrical nerve stimulation, which applies electrical current to the skin through electrodes, can achieve therapeutic effects such as pain relief [12]. However, the complex electromagnetic parameters of biological tissues make it challenging to achieve precise stimulation of deep target areas due to the diffuse distribution of the stimulation current in the tissue [13]. Techniques like deep brain stimulation involve the direct implantation of DBS leads into the target area and the application of electrical current, enabling precise stimulation of the target area. It has proven to be an effective method for treating epilepsy and depression [1]. However, the implantation of electrode during surgery can cause mechanical stress and potential damage [14]. The use of external connecting wires also carries the risk of infection and inflammation [15]. Additionally, the limited battery capacity and its impact on patient mobility are additional limitations [16]. Wireless neuroregulation techniques, such as transcranial magnetic stimulation, utilize focused pulsed magnetic fields to induce electric currents in the tissue, thereby exciting or inhibiting the target nerves and achieving neuroregulation. These techniques are commonly used in the treatment of psychiatric disorders or for memory improvement. Research in this field has focused on improving the focusing of the magnetic field through modifications in coil design [17–19] and adding focusing devices such as conductive or magnetic conductive baffles [20]. However, the dispersion of the magnetic field makes it difficult to achieve millimeter-level focusing of the induced electric field, often resulting in simultaneous stimulation of adjacent brain regions. Wireless magnetic stimulation based on coils also faces challenges such as rapid magnetic field attenuation, maximum electric field intensity at the skin surface, and difficulty reaching deep brain regions [21, 22]. With advancements in brain mapping and the refinement of functional brain regions [23], our understanding of stimulation mechanisms has improved, and precise stimulation has become crucial for ensuring the effectiveness of stimulation [21]. Therefore, the development of new high precision neural magnetic stimulation methods that achieve millimeter-level precision and minimize trauma is an urgent issue in the field of magnetic stimulation [24, 25].

Some research groups have proposed various methods for neural stimulation. These groups have achieved wireless stimulation of peripheral nerves, such as the blood vessels surrounding the nerves and the sciatic nerve of animals, by creating millimeter-level electronic implants. These implants transmit energy wirelessly through coils, ultrasound, magneto-electric materials, or by harnessing frictional energy [26–29]. However, the implantation of electronic devices still faces challenges, such as the risk of surgical manipulation, as well as the risk of infection associated with hard electrodes incompatibility and long-term foreign body implantation [14, 30]. A study utilized soft capacitive conductive hydrogels as implantable stimulators. This approach minimizes the risk of inflammation due to mechanical stress by using fully biodegradable and biocompatible circuit components and substrates to construct wireless stimulators. However, it still requires the use of coils to transmit power to the battery [31]. Kozielski et al. proposed a direct injection of magneto-electric nanoelectrodes into the subthalamic nucleus of mice. These nanoelectrodes can respond to external magnetic fields and wirelessly transmit electrical signals to the brain, thereby regulating the mice's movement speed [32]. However, this method requires the application of alternating magnetic fields in a static magnetic field, and there is still room for improvement in the difficulty and convenience of equipment manufacture from clinical application.

In the theory of electromagnetic fields, it has been observed that the interface between a high conductivity medium and biological tissue under alternating magnetic fields can accumulate charges and generate a focused electric field that is higher than the induced electric field itself [33]. This study aims to take advantage of this property to achieve millimeter-level precise wireless neural magnetic stimulation in target areas. This is done by using high conductivity implants that are implanted in the target area through minimally invasive techniques and stimulated by an external electromagnetic field. This puts forward high requirements for the electrical conductivity, softness and biocompatibility of the materials of the implants. In recent years, emerging gallium-based

LM materials have emerged as a promising choice for focused stimulation implants [34, 35]. These materials exhibit high conductivity, flexibility, and good biocompatibility. They have found wide applications in fields such as injectable biomedical technologies and neuroscience as neural prostheses, implanted flexible electrodes, and contrast agents [36–38]. Numerous studies have confirmed their feasibility and safety for long-term implantation in neural sites [34, 39]. The 8-coil is a commonly used stimulation coil in neuroregulation. It can induce a focused vector electric field. In this study, a pulsed magnetic field generated by a pulsed current was applied to the 8-coil to induce the LM implant to produce a locally focused electric field on the order of millimeters. As a result, precise magnetic stimulation of the surrounding nerves is achieved, leading to a significant improvement in the effectiveness of magnetic stimulation.

## Principle

### Principle of magnetic stimulation based on 8-coil and LM

According to the principle of current magnetic effect and electromagnetic induction, a high-voltage pulse current is used to pass through the coil to generate an induced magnetic field, which in turn produces an electric field in the nerve tissue, thereby changing the nerve activity. The distribution of the induced electric field generated by a current carrying coil can be calculated using Biot-Savart's law, which describes the relationship between the magnetic field and the current element dl in a closed wire.

$$A = \frac{\mu_0}{4\pi}\int_L \frac{I(t)}{r} dl \#2\text{-}1$$

$Where\ dl = dl_x \cdot i + dl_y \cdot j + dl_z \cdot k$ , $r = r_x \cdot i + r_y \cdot j + r_z \cdot k$, $\mu_0$ represents the vacuum permeability, $L$ is the integral path along the current element on the coil, and r is the distance from any point P in space to the current source $dl$. The induced electric field $E$ generated by the time varying current is then given by:

$$E = \frac{\partial I(t)}{\partial t}\frac{\mu_0}{4\pi}\int_L \frac{1}{r} dl \#2\text{-}2$$

Referring to the commonly used 8-coil design in magnetic stimulation [40], it comprises two circular coils combined to generate a focused vector-induced electric field. The electric field strength is the superposition of the two circular coils, as depicted in Fig. 1(a). Boundary conditions at the interface between two media, 1 and 2, can be summarized as:

$$\begin{cases} \mathbf{a}_n \times (\mathbf{E}_1 - \mathbf{E}_2) = 0 \\ \mathbf{a}_n \times (\mathbf{H}_1 - \mathbf{H}_2) = \mathbf{J}_s \\ \mathbf{a}_n \cdot (\mathbf{D}_1 - \mathbf{D}_2) = \rho_s \\ \mathbf{a}_n \cdot (\mathbf{B}_1 - \mathbf{B}_2) = 0 \#2\text{-}3 \end{cases}$$

In this context, $\boldsymbol{a}_n$ denotes the unit normal vector to the interface pointing towards medium 1, while $\boldsymbol{\rho}_s$ and $\boldsymbol{J}_s$ represent the surface charge density (C/m²) and surface current density (A/m) on the interface, respectively. Let $\boldsymbol{E}_T$ be the induced electric field generated by the 8-coil setup at a certain moment, and $\boldsymbol{\rho}_{sT}$ be the charge density. Assuming the induction electric fields at the junctions of the LM with neural tissue along the y-axis and x-axis are $\boldsymbol{E}_{n1}$ and $\boldsymbol{E}_{n2}$ respectively, as illustrated in Fig. 1(b). From Eqs. 2–3, it follows that along the tangent direction to $\boldsymbol{E}_T$ (i.e., along the x-axis at the boundary with tissue), the electric field is perpendicular to $\boldsymbol{E}_T$, yielding a dot product of 0. Conversely, along the direction perpendicular to $\boldsymbol{E}_T$ (i.e., along the y-axis at the

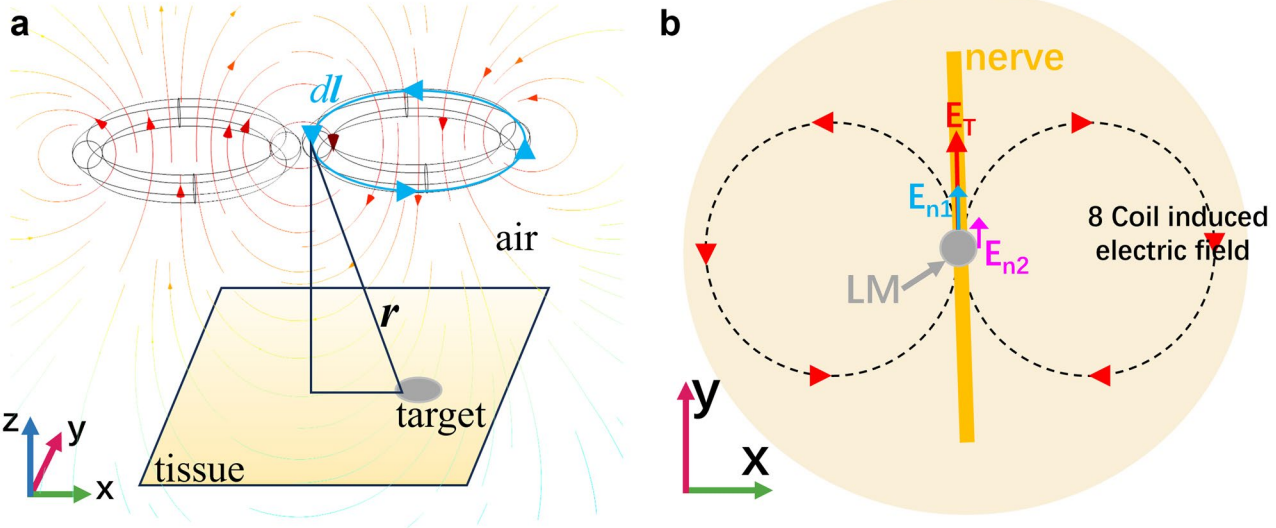


**Fig. 1** Schematic diagram of how LM generate electric fields in magnetic field. (**a**) Schematic diagram depicting the induction current induced by the energized coil at the target tissue site. (**b**) Schematic diagram illustrating the induced electric field generated in LM under 8-coil excitation

boundary with tissue), charge accumulation occurs, leading to:

$$\boldsymbol{a}_n \cdot \boldsymbol{E}_{n1} = \boldsymbol{\rho}_{sT}, \ \ \boldsymbol{a}_n \cdot \boldsymbol{E}_{n2} = 0 \#2\text{-}4$$

From Eqs. 2–4, the induced electric field by the 8-coil setup is influenced by the presence of LM. This results in charge accumulation along the y-axis at the boundary with tissue, while no charge accumulates along the x-axis. Due to the significantly higher electrical conductivity of LM compared to biological tissue, the charge density $\boldsymbol{\rho}_{sT}$ induced by the 8-coil setup at the boundary with LM along the y-axis is higher than that induced by the 8-coil setup in biological tissue. The superposition of these two induced electric fields results in a high amplitude induced electric field. It is indicating that under the action of the pulsed magnetic field from the 8-coil setup, a vector stimulation electric field can be formed along the y-axis, while the electric field intensity along the x-axis decreases. Additionally, due to shielding effects, the amplitude of the induced electric field below the coverage area of the LM will also decrease.

Finite element analysis was used in this study to simulate the electric field distribution induced by stimulation coils containing LM. A biological tissue model confirmed the theoretical predictions of electromagnetic fields. We then employed an 8-coil setup and a high-voltage pulse generator to create magnetic field, and we measured the induced electric field distribution in our experimental model. Comparisons of the electric fields, with and without LM, validated the enhancement of millimeter-level stimulation regions by LM. Lastly, we stimulated the sciatic nerves of mice, recording EMG responses from the gastrocnemius muscle and leg movement amplitudes to assess the focal and enhancing effects of LM.

## Materials and methods

### Liquid metal

In this experiment, $Ga_{67}In_{20.5}Sn_{12.5}$ LM, purchased from Suzhou Haichuan Metal Products Co., Ltd., was utilized. Its pertinent physical properties include a melting point of 10.5 ℃, electrical conductivity of $3.4 \times 10^6$ S/m, density of 6.5 g/cm³, viscosity of 2.98 mPa·s, and surface tension of 0.533 mN/m [34]. In a biological environment, it exists in a liquid state with a conductivity much higher than that of conductive hydrogels. It possesses characteristics such as flexibility, good biocompatibility, and stretchability. Considering implantation feasibility and safety, approximately 0.65 g, or about 1 µL, of LM was chosen for implantation, as depicted in Fig. 2(a).

### 8-coil, pulse current generator and electric field distribution measurement method

The 8-coil setup and high voltage pulse current generator used in this study were developed by the Institute of Biomedical Engineering, Chinese Academy of Medical Sciences. The pulse magnetic field generated had a pulse width of 280 µs. The induced magnetic field distribution of the 8-coil setup was measured using a gaussmeter (Model 475 DSP, Lake Shore) (Supplement Fig. S3). Pulse stimulation is a sine wave in both directions (Supplement Fig. S4 for images of magnetic field measurements for high energy magnetic stimulation), therefore, we believe that there will be no charge accumulation or polarization on the surface of the LM that could affect the stimulation effects.

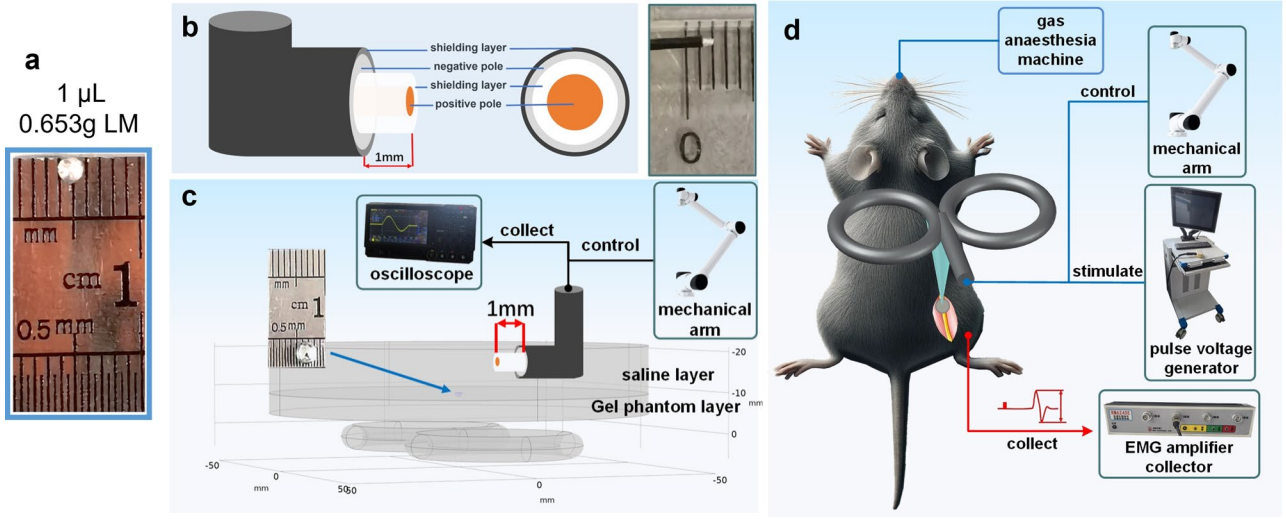


**Fig. 2** Schematic of the Methodology. (**a**) Volume and morphology of 1 µL LM. (**b**) Schematic and actual image of the induction electric field measurement probe.(**c**) Schematic of the induction electric field measurement experiment.(**d**) Schematic of LM stimulating the sciatic nerve of mice

Due to the difficulty in directly measuring the induced electric field distribution in tissue, we designed a gel phantom-saline water-LM model to validate the simulation and theoretical results. The gel phantom has a conductivity of approximately 1 S/m, while the saline has a conductivity of 0.9 S/m. A coaxial line was used as a vector electric field measurement probe, which effectively shields the induced current generated by the magnetic induction in the measurement probe [41]. The schematic and physical diagrams of the measurement probe are shown in Fig. 2(b). The measurement probe was controlled by a mechanical arm to measure the electric field distribution in the saline. Based on this, the stimulation current generated by the coil and LM in real tissue was reflected. The simulated distribution of the induced electric field generated by the LM was calculated and verified through actual measurements. The schematic diagram of the measurement principle is shown in Fig. 2(c).

### Finite element simulation

Finite element analysis was conducted using COMSOL Multiphysics 6.0 software, specifically within the electromagnetic module, to simulate the distribution of induced electric fields caused by LM and biological tissues in alternating magnetic field. The 8-coil, biological tissue model, and LM models were established, as depicted in Fig. 3(a). The biological tissue was modeled as a cylinder, 15 mm in radius and 80 mm in length, comprising soft tissue, skin, and bone. Nerve tissue was similarly modeled as a cylinder, but with a 1 mm radius and an 80 mm length. LM was represented by a semicircular droplet with a 0.25 mm radius. Electrical conductivities were assigned as follows: soft tissue at 0.2 S/m, skin at 0.31 S/m, bone at 0.006 S/m, nerve tissue at 1.79 S/m, and LM at 3 × 10^6 S/m [42]. The parameters of the 8-coil setup included two parallel circular loops with large radii of 20 mm and small radii of 5 mm, defining the tangent at the intersection of the two coils as the y-axis coordinate, corresponding to the x and z axes, as shown in Fig. 3(b). The initial stimulation parameters of the coil included a frequency of 3000 Hz, current of 1000 A, and 7 turns. Tetrahedral meshing was employed, resulting in 572,548 mesh elements with an average element quality of 0.6224.

### Collecting EMG signals evoked by stimulating the sciatic nerve

In this study, C57BL/6J mice were purchased from Huafukang Biotechnology. At the time of the acute anesthesia experiment, the mice were anesthetized using 2% isoflurane (RWD) and 2 L/min oxygen with a respiratory anesthesia machine (R580S, RWD). The mice were kept under shallow anesthesia for at least 20 min to ensure a

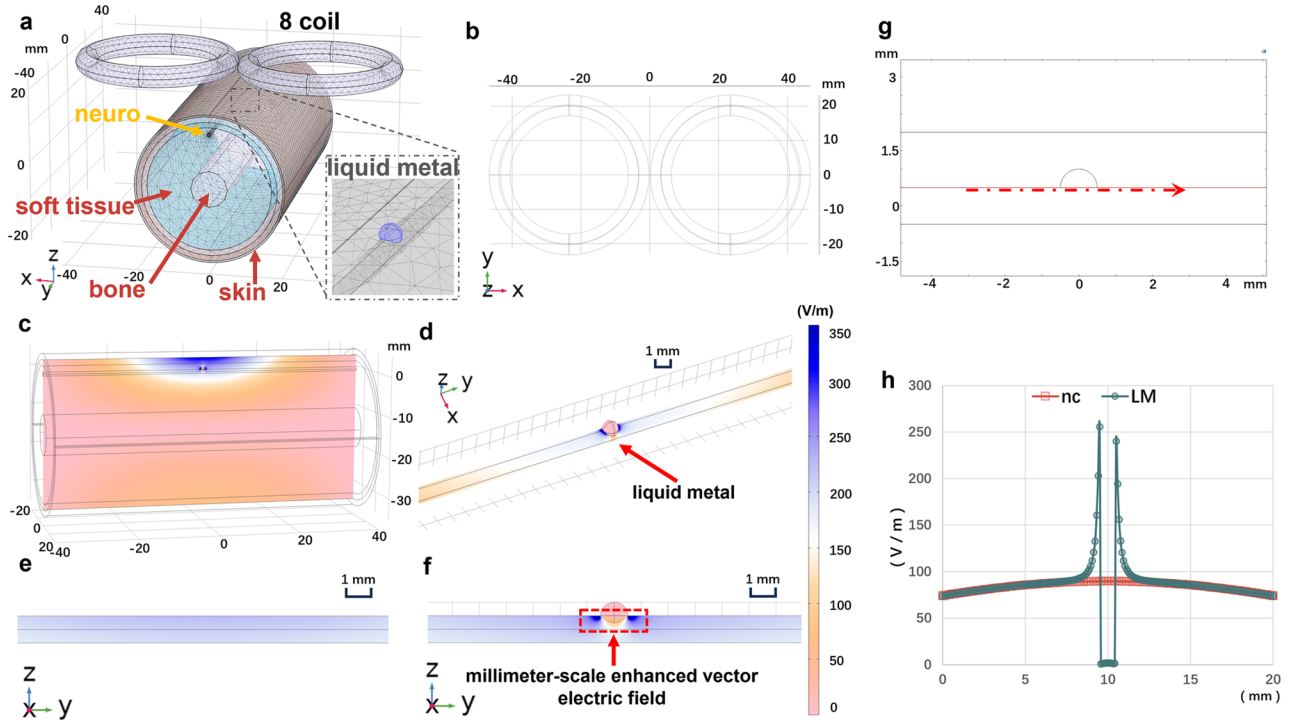


**Fig. 3** LM-Tissue-Nerve stimulation model. (**a**) Mesh partition diagram of the simulation model. (**b**) Definition of the 8-coil and coordinate axes. (**c**) Cross sectional view of the induced electric field distribution along the yz-axis. (**d**) Induced electric field distribution in nerve tissue and LM. (**e**) Induced electric field distribution without LM control. (**f**) Induced electric field distribution with LM. (**g**) Tangential schematic. (**h**) Comparison of induced electric field amplitude distribution along the tangential line (**g**)

stable state before measurements were taken. The LM was weighed and then sterilized using ultraviolet light (30 min). It was subsequently placed in PBS solution and directly injected into the sciatic nerve region using a syringe. Silver wire electrodes were implanted into the mice's gastrocnemius muscle, with the signal electrode connected to the stimulated side of the muscle, the reference electrode attached to the contralateral gastrocnemius, and the ground electrode connected to the mouse's tail. Data were collected using an RM6240E instrument from Chengdu Instrument Factory, with a sampling rate of 100 kHz and a bandpass filter with a range of 0.8 Hz to 1 kHz. The principle is illustrated in Fig. 2(d). CT scans were performed to evaluate the status of the mice after the implantation of the LM using Mediso - nanoScan® CT system.

The spatial positioning of both the 8-coil setup and the electric field distribution measurement probe was controlled using the HAN'S ROBOT company's P03 mechanical arm. This facilitated variable control of coil spatial positions and scanning measurement of induced electric field distribution. The positioning accuracy of the mechanical arm was maintained at 0.1 mm (Supplement Fig. S5).

## Results

### Finite element simulation of millimeter-level vector electric field focusing area induced by Lm in neural tissue

The induced electric field triggered by the magnetic field generated by the 8-coil is the superposition of induced electric fields along three axial directions, with the highest proportion from the y-axis direction. This characteristic results in a vector electric field along the y-axis induced by the 8-coil stimulation. The simulated induced electric field of the 8-coil is shown in Supplement Fig. S1, where the proportions of x-axis and z-axis components are minimal on the same coordinate scale. Previous studies have indicated that the stimulation effect in actual stimulation is primarily governed by the vector stimulation along the y-direction. Therefore, all simulated electric field results obtained below in this paper focus solely on the y-axis direction components.

The distribution of induced electric fields from LM wireless stimulation is shown in Fig. 3. The 8-coil induces induced electric fields in tissue and neural, with the induced electric field distribution along the yz-axis as depicted in Fig. 3(c). The focusing electric field region induced by LM is illustrated in Fig. 3(d), while the distributions of induced electric fields before and after the addition of LM are shown in Fig. 3(e) and 3(f), respectively. Simulation results indicate the generation of induced electric fields in tissue and neural under 8-coil stimulation. Upon the addition of LM, significant focusing electric fields are generated on both sides of the LM along the y-axis of the coil, while the electric field amplitude decreases on both sides of the x-axis and below the LM coverage area, consistent with theoretical analysis results.

The comparison of induced electric field distributions along the tangent to the interface between the neural y-axis and LM, as shown in Fig. 3(g), demonstrates the contrasting results of induced electric field distribution, as illustrated in Fig. 3(h). Two millimeter-level focusing electric fields are generated on both sides of the y-axis of the LM, with a significant increase in electric field amplitude. Consequently, the focusing induced electric field induced by LM can precisely stimulate specific target points on neural tissue.

### Finite element simulation and field distribution measurement of millimeter-level vector electric field focusing area generated by Lm in gel-saline water

To validate the simulation and theoretical results, we conducted simulations and actual measurements on a gel phantom-saline water-LM model. The simulation model, as shown in Fig. 4(a), (b), and (c), respectively measures along the x, y, and z axes of the LM, with schematic diagrams of the measurement paths. To facilitate measurements and minimize discrepancies between the actual model and simulation, a hemispherical solid LM was fabricated and placed in the gel phantom at temperatures below the melting point of the LM. The validation model schematic is depicted in Fig. 2(d). Simulation results are shown in Fig. 4(d), (e), and (f), while measurement results are illustrated in Fig. 4(g), (h), and (i). The results indicate the formation of millimeter-level focusing electric fields along the y-axis of the LM, with a decrease in electric field intensity along the x-axis direction and within the LM coverage area. The simulation results are consistent with the measured trends. Discrepancies between simulation and measurement results mainly stem from differences between the actual 8-shaped coil used and the ideal circular coil in the simulation. Additionally, the spacing between the positive and negative poles of the measurement probe is 1 mm, leading to errors in the voltage difference obtained compared to the numerical calculation results, partly due to magnetic field interference through spatial coupling.

### LM Precision stimulation of mouse sciatic nerve for eliciting EMG

Considering the volume of LM and safety assessments from previous studies, 1 μL of LM was placed on the mouse sciatic nerve. EMG corresponding to the gastrocnemius muscle and leg movement amplitude were measured and compared between the nc group and the LM group (Supplement Fig. S2). Using an 8-coil, pulses of 410 V to 470 V were applied, resulting in a corresponding

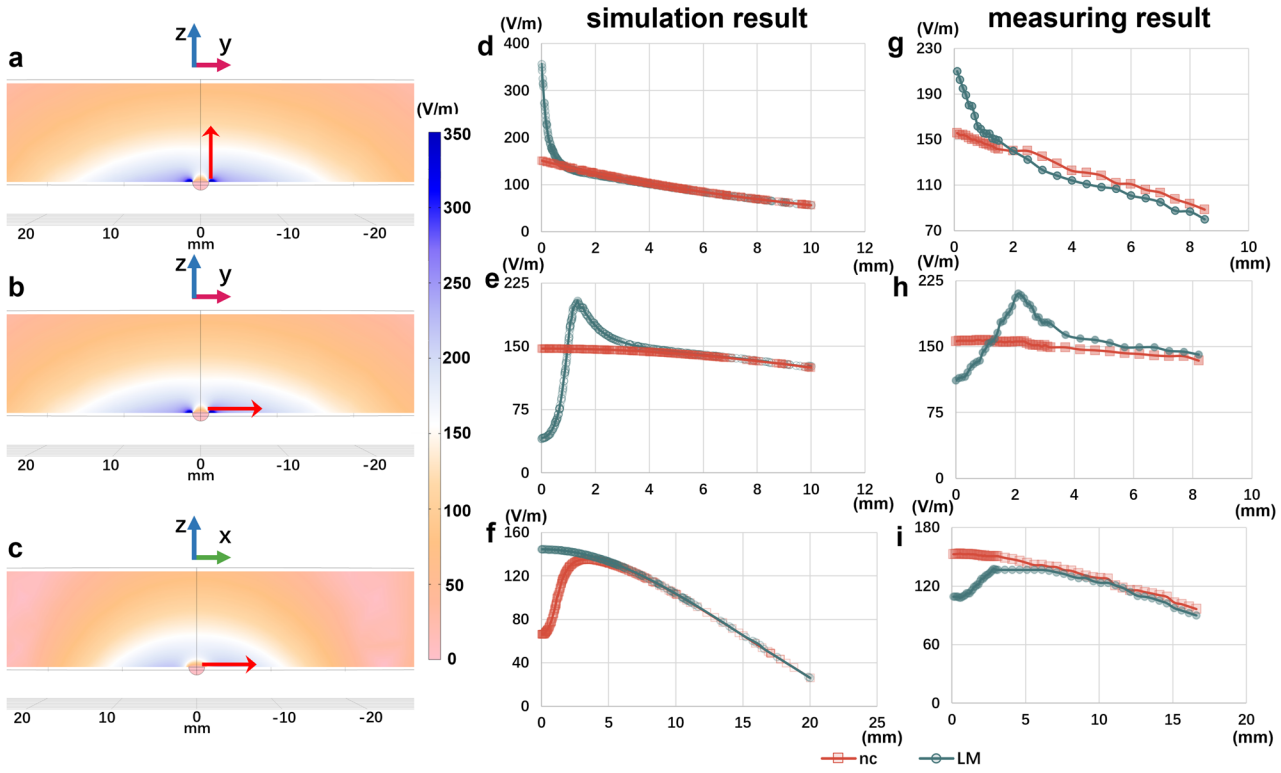


**Fig. 4** Electric field amplitude measurements and simulation results. (**a**), (**b**), and (**c**) represent cross sectional views of LM-Tissue-Nerve stimulation model electric field distribution along the yz, yz, and xz axes, respectively. (**d**), (**e**), and (**f**) correspondingly compare the simulated induced electric field distributions between the nc group and LM group along the directions of the red lines in (**a**), (**b**), and (**c**). (**g**), (**h**), and (**i**) present the measured induced electric field distributions comparing the nc group with the LM group along the directions of the red lines in (**a**), (**b**), and (**c**), respectively.

pulse magnetic field of approximately 0.4–0.45 T on the sciatic nerve. The measured EMG amplitudes are shown in Fig. 5(a), with the corresponding box plot depicted in Fig. 5(b). For processing the EMG signals, a threshold of greater than 0.1 mV was established as an effective signal. Since EMG signals in the NC group were difficult to observe at voltages below 410 V, we selected 410 V as the initial collection voltage. At this voltage, the EMG signal amplitude in the LM group was significantly higher than that in the NC group. This indicates that the minimum stimulation voltage required to evoke EMG signals in the LM group is clearly lower than 410 V, suggesting that LM wireless magnetic stimulation significantly enhanced both the stimulating electric field and the associated muscle response. At 460 V voltage, the corresponding mouse leg movement amplitude comparison is shown in Fig. 5(c), with the corresponding video material available in supplement video. To evaluate the focusing stimulation effect of the LM, we placed the LM on one side of the nerve, as shown in Fig. 5(d). The statistical results of the corresponding EMG amplitudes under the same magnetic field are shown in Fig. 5(e). There is a significant difference in the EMG induced by the LM at positions 1 and 2, while there is no significant difference between position 2 and the nc group. These results indicate that the focusing electric field induced by the LM is concentrated only on the y-axis side of the coil. Shifting the LM by 2 mm does not significantly change the stimulation effect, indicating that the precision of the stimulation field reaches the millimeter-level. Under a pulsed magnetic field of approximately 0.45 T, the EMG amplitude is increased by approximately 500%. The data presented in this study were obtained under relatively strict control of variables. The values of $n = 10$ and $n = 20$ mentioned in Fig. 5 represent the EMG amplitude results obtained from multiple stimulations of the same mouse during a stable anesthetic window at a fixed dose. This approach ensured stable anesthesia and consistent electrode placement for EMG recording. Additionally, a robotic arm was used to precisely control the coil position, maintaining a stable relative position between the coil, LM, and the nerve.

Figure 6 shows the CT scan and cross-sectional images of the sciatic nerve in mice 7 days after LM injection. The CT images of day0 and day7 and the status map of the LM on the day7 are shown in Supplement Fig. S6. To evaluate the safety of LM injection, four additional mice were selected for a four-week study. Unlike the acute anesthesia experiments, no invasive procedures were performed in the long-term study. 1 μL of sterilized LM

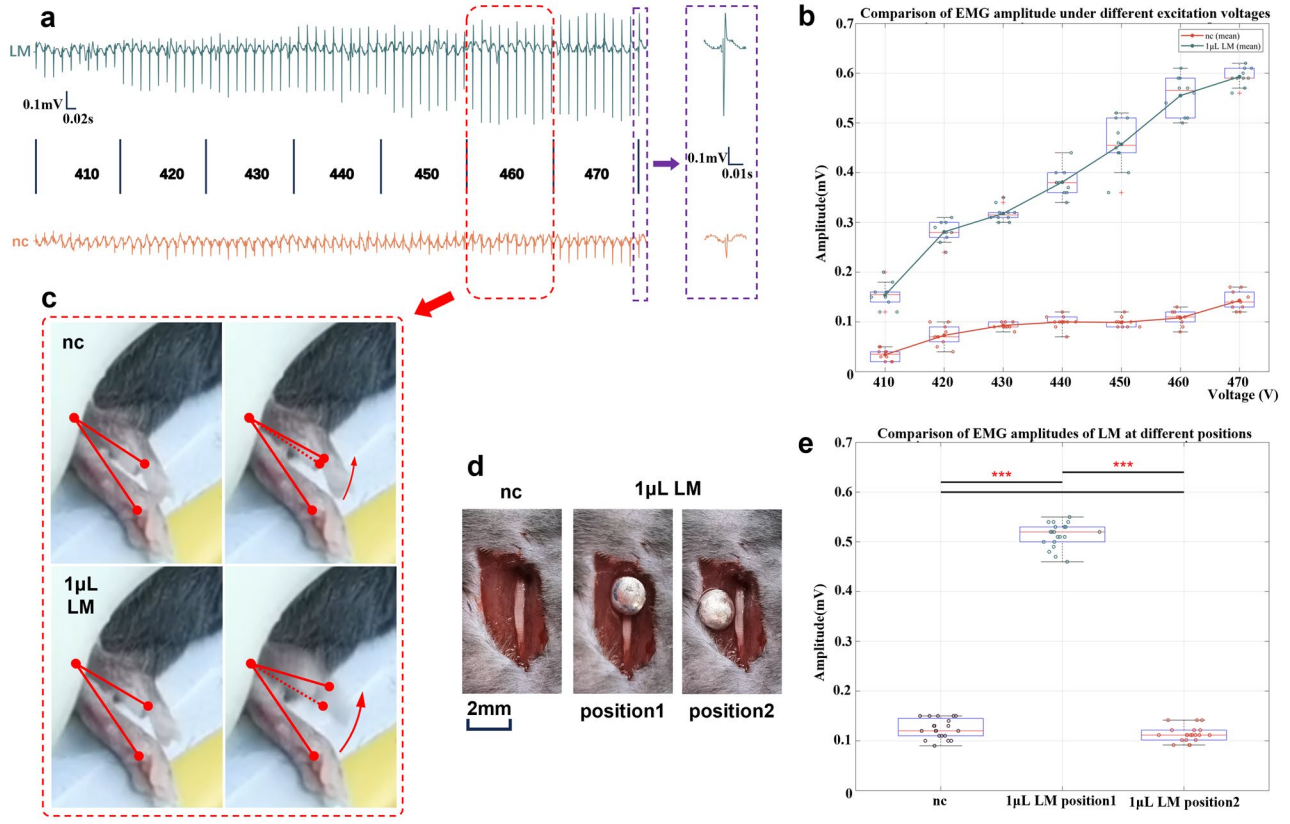


**Fig. 5** Precision Stimulation of Mouse Sciatic Nerve to Evoke EMG with LM. (**a**) Comparison of EMG amplitudes between the nc group and LM group at different stimulation voltages. (**b**) Box plots of EMG amplitudes between the nc group and LM group at different stimulation voltages, with $n = 10$. (**c**) Amplitude of leg movement evoked in mouse gastrocnemius muscle by the nc group and LM group under the same magnetic field. (**d**) Experimental setup for LM stimulation at different positions. (**e**) Comparison of EMG amplitudes evoked by LM at different positions and between the LM group and nc group under the same magnetic field, $n = 20$, ***: $p < 0.001$

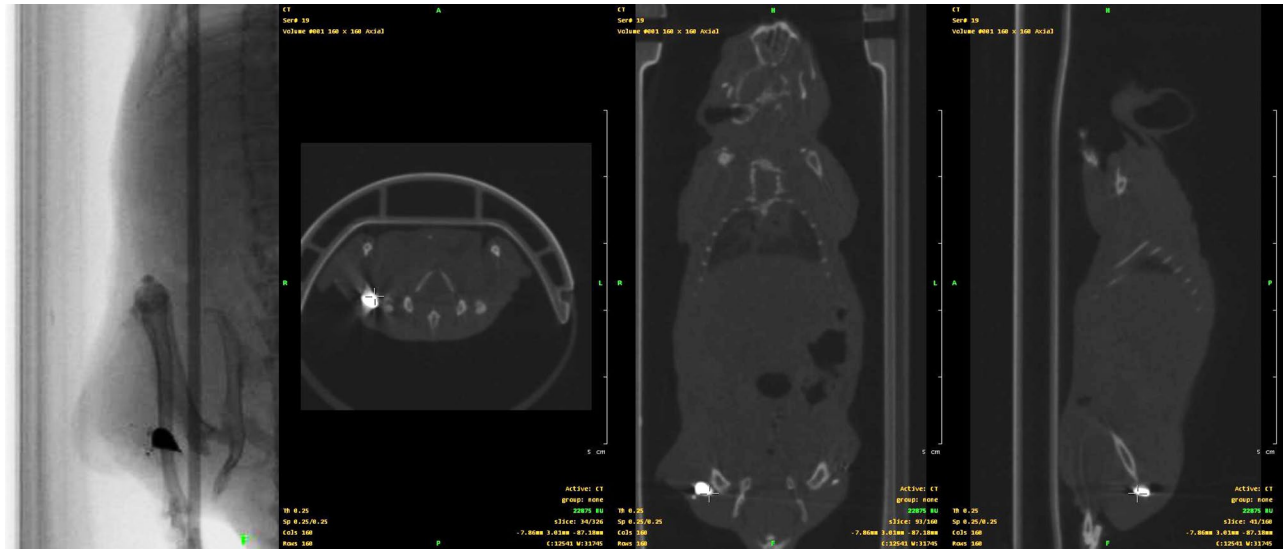

**Fig. 6** CT scan images and cross-sectional views of the sciatic nerve in LM-implanted mice after 7 days

was directly injected onto the sciatic nerve site, another group of four mice injected with an equal volume of PBS served as the nc group, followed by anesthesia and magnetic stimulation every 7 days. The results showed a 100% survival rate in all mice. Over the four weeks, no significant differences were observed between the experimental and nc groups in locomotion, food intake, water consumption, or body weight.

## Discussion

When we consider LM as a stimulating electrode, our proposed technique offers a new approach for implantable magnetic stimulation. Flexibility enables the LM to be injected non-surgically between the nerve and muscle. This approach might be more readily accepted by patients both psychologically and physiologically. The excellent electromagnetic properties of LM allow it to be wirelessly stimulated, eliminating the need for electrode connections or built-in batteries, and thus facilitating neural activation at the target site. Additionally, LM is able to remain in a agglomerated droplet shape after injection, giving it superior focusing capabilities compared to dispersed magnetic nanoparticles. The increase in stimulation intensity means that LM can counteract the rapid decay of the magnetic field from the magnetic stimulation coil to some extent, enhancing stimulation depth. The precise stimulation method can be applied to peripheral nerve stimulation, and the millimeter-level precision and depth of magnetic stimulation is of great significance for precise mapping of the brain through magnetic stimulation. Therefore, achieving millimeter-level precise control of the brain is a goal we hope to further pursue in the future.

Compared to the method of directly injecting LM into the target, this approach is more convenient than implanting tiny electronic circuit stimulators. Due to the high density of LM, low doses of X-ray technology may be used for imaging assistance [43]. This study demonstrates that highly conductive media enable millimeter-scale focused magnetic stimulation. Further analysis and experimental validation are needed to quantify the effects of other parameters, such as the morphology and volume of LM, on stimulation outcomes. The key factors influencing the EMG results include the mouse's anesthesia state, electrode placement, magnetic field strength, and the relative positions of the LM, coil, and nerve. Even with constant parameters, such as coil position, stimulation voltage, and anesthetic dosage, variability in EMG signals was observed for the same mouse. Therefore, precise quantitative relationships, such as the enhancement of electromyography under different magnetic field strengths, potential changes in stimulation effects caused by muscle deformation during movement, and individual differences between subjects, require further investigation. Experiments conducted on multiple mice consistently showed similar EMG amplitude enhancement. However, variations in anesthesia states and electrode placement between mice limited the statistical comparability. The main objective of this study is to generate millimeter-scale electric fields with the highest amplitude. The intensity and volume of the focused electric field are mutually constrained; as the LM volume decreases, the focus region becomes smaller, leading to more precise stimulation, but the total energy and stimulation intensity decrease. Therefore, the selection of LM volume for different stimulation areas (e.g., larger brain regions or sub-neural bundle regions) requires further experimental validation. Future efforts will focus on minimizing the influence of variables, such as anesthesia state, by standardizing factors like the volume and morphology of the implanted LM, as well as mouse weight, sex, age, electrode positioning, and the relative alignment of the nerve and coil. Better control of these variables will improve the accuracy of quantitative statistical results and enable more reliable comparisons between different subjects.

In the method proposed in this study, the relative position of the LM to the nerve is a crucial factor affecting the efficacy of stimulation. Firstly, the magnetic field does not induce a change in the relative position of the LM because we utilize a magnetic field consisting of microsecond pulses with relatively low total energy. Additionally, the LM has a low magnetic susceptibility, which means that it does not deform and move as a result of being forced by the magnetic field [44]. During stimulation in air, we did not observe any measurable changes in morphology. Furthermore, related studies have confirmed that LM will remain stable in the biological environment. Evaluations of the morphology, position, and safety of LM post-injection indicate that there were no observable changes in the position or morphology of the LM even after 60 days post-injection. Additionally, the Ga content in organs post LM implantation showed negligible increase, providing further evidence for the safety of LM in vivo [45]. Because the viscosity of the LM is similar to that of the water, when filling into the biological tissue, the material would conformably be attached to the tissues. During LM implantation, CT scans and anatomical observations showed that its relative position to the nerve remained largely unchanged. Although muscle tissue deformation induced by movement may lead to slight changes in LM shape, there will be no significant alteration in the relative position between the coil and the nerve. Regarding the potential safety concerns of LM particles loosening or splitting due to movement, it is inevitable that small amounts of LM may enter the bloodstream. For these trace amounts of dispersed LM, numerous studies involving direct in vivo injection of the

materials provide evidence of their safety in experimental animals. Examples include dispersed LM-based nanomaterials for tumor ablation and CT-enhanced imaging [46], and dispersed LM microparticles for improving hydrogel conductivity [47]. LM particles can be excreted through urine or feces [48]. Analysis of LM content in organs and blood provides evidence for the safety of LM implantation.

Although many studies have demonstrated the safety of LM for injectable medical applications, this method incorporates an external magnetic field, introducing unique considerations for LM's redox reactions in vivo. First, the focused electric field decays within 1 mm, and the dynamic voltages generated for neuroregulation are lower than LM's redox potential. Second, the stimulation used in this study involved short pulses at a 2 Hz repetition rate, which introduced less energy compared to approaches using LM directly as a stimulation electrode, further supporting the safety of this method. Regarding potential oxidation and reduction reactions caused by surface oxide layer disruption during muscle movement, these processes could lead to thickening of the oxide layer. With increased oxidation, LM may become stickier, enhancing tissue wettability. However, an overly thick oxide layer could reduce LM conductivity and weaken the stimulation effect [49]. The results show that the increase in oxide layer thickness was not significant at Day 7. These findings provide preliminary evidence supporting the safety of LM under external magnetic field.

Wireless magnetic stimulation inducing induced currents in LM inevitably leads to thermal effects. These thermal effects will be greater in high conductivity LM than in tissue. Thermal effects can also excite neural tissues. However, due to the instantaneous nature of pulsed magnetic field, it is difficult to measure in real-time. Additionally, cumulative thermal effects from continuous pulsing cannot reflect whether instantaneous thermal effects play a role in neuroregulation. Hence, in the next step, we hope to investigate the role of thermal effects in neuroregulation through simulation calculations or suitable control experiments.

In comparison to research on magnetic nanoparticles enhancing stimulation effects, magnetic nanoparticles can achieve external static magnetic field control, aggregate nanoparticles, target specific areas, alter target area magnetic properties, increase induced magnetic field intensity, and thus induce stimulation. In contrast, the method of injecting LM is based on altering the electrical properties of the target area to induce changes in induced electric field intensity. This method is advantageous due to its straightforward operation and the limited dispersion of LM. However, LM has magnetic properties nearly identical to biological tissue, thus it scarcely alters the magnetic field distribution, nor does it easily allow for external control of LM's spatial positioning. Consequently, employing specific magnetic materials to create magnetic LM, and capitalizing on the benefits of both electrical and magnetic characteristics, could potentially refine the electric field distribution through adjustments in the magnetic field. Controlling LM movement via an external static magnetic field [50], along with potential effects such as magnetic heating [51], might enhance stimulation outcomes. This constitutes an important area for further research [52].

## Conclusion

LM generates millimeter-level focused induced electric fields within the pulsed magnetic field of an energized coil. Leveraging this characteristic holds the promise of achieving minimally invasive, wireless, and precise neural stimulation with implanted LM. In this study, the distribution pattern of the induced electric field at the interface between LM and tissue under an 8-coil configuration was theoretically derived and validated through finite element simulation analysis. The reliability of the theoretical derivation and simulation was further confirmed by practical measurements using a saline gel model. Finally, basic validation of the proposed method was achieved through the stimulation of the mouse sciatic nerve-gastrocnemius muscle model implanted with LM. The results show that under the excitation of 8-coil, the LM generates a millimeter-scale focused vector-induced electric field, significantly enhancing the stimulation effects on the mouse gastrocnemius muscle movement and electromyography. This provides preliminary evidence for the safety of in vivo implantation of LM under an external magnetic field.

## Supplementary Information

The online version contains supplementary material available at https://doi.org/10.1186/s12984-025-01575-2.

Supplementary Material 1

Supplementary Material 2

**Acknowledgements**

We thanks to Prof. Jinjian Liu for his valuable guidance in the process of CT photography.

**Author contributions**

Y.W. carried out the experiment, analyzed the data, and wrote the manuscript. X.W., J.L., K.Z., X.M., R.W., F.C. and M.W. gave guidance on animal experiments. R.M., X.L., W.M., R.L. and Y.N. gave guidance on COMSOL programming. J.W. and J.J. gave guidance on the magnetic field generating device. S.Z., Z.L. and T.Y. oversaw all of the research phases and revised the manuscript.

**Funding**

This work was supported by National Natural Science Foundation of China 81927806, CAMS Innovation Fund for Medical Sciences（CIFMS）2023-I2M-QJ-017, Tianjin Multiple Investment Project of Application Foundation 21JCYBJC00870 Fundamental, Research Funds for the Central Universities

3332023073 and National Natural Science Foundation of China Basic Research Project for Young Doctoral Students 823B2028.

**Data availability**
The data are available from the corresponding author on reasonable request.

## Declarations

**Ethics approval and consent to participate**
This study was approved by the Ethics Committee of the Institute of Radiation Medicine, Chinese Academy of Medical Sciences (IRM/2-IACUC-2406-018).

**Consent for publication**
All the authors provided their consent for publication of the present version of the manuscript.

**Competing interests**
The authors declare no competing interests.

Received: 28 May 2024 / Accepted: 11 February 2025
Published online: 07 April 2025

**References**

1. Lozano AM, et al. Deep brain stimulation: current challenges and future directions. Nat Reviews Neurol. 2019;15(3):148–60.
2. Resende L, et al. Meta-analysis of transcutaneous electrical nerve stimulation for relief of spinal pain. Eur J Pain. 2018;22(4):663–78.
3. Hallett M. Transcranial magnetic stimulation: a primer. Neuron. 2007;55(2):187–199.
4. Boon P, De Cock E, Mertens A, Trinka E. Neurostimulation for drug-resistant epilepsy: a systematic review of clinical evidence for efficacy, safety, contraindications and predictors for response. Curr Opin Neurol. 2018;31(2):198–210.
5. Loo CK, et al. International randomized-controlled trial of transcranial direct current stimulation in depression. Brain Stimul. 2018;11(1):125–33.
6. Fisicaro F, et al. Repetitive transcranial magnetic stimulation in stroke rehabilitation: review of the current evidence and pitfalls. Ther Adv Neurol Disord. 2019;12:1756286419878317.
7. Kathe C, et al. The neurons that restore walking after paralysis. Nat Vol. 2022;611(7936):540–7.
8. Zeng Z, Yang Y, Deng J, Saif Ur Rahman M, Sun C, Xu S. Physical stimulation combined with biomaterials promotes peripheral nerve injury repair, repair. Bioengineering. 2022;9(7):292.
9. Han F, et al. Strategy for Designing a Cell Scaffold to Enable Wireless Electrical Stimulation for enhanced neuronal differentiation of stem cells. Adv Healthc Mater. 2021;10(11):2100027.
10. Cohen SP, Vase L, Hooten WM. Chronic pain: an update on burden, best practices, and new advances. Lancet. 2021;397(10289):2082–97.
11. Gibson W, Wand BM, Meads C, Catley MJ, O'Connell NE. Transcutaneous electrical nerve stimulation (TENS) for chronic pain-an overview of Cochrane Reviews. Cochrane Database Syst Reviews. 2019;4
12. Dailey DL, et al. Transcutaneous electrical nerve stimulation reduces movement-evoked pain and fatigue: a randomized, controlled trial. Arthritis Rheumatol. 2020;72(5):824–36.
13. Johnson MI. Resolving long-standing uncertainty about the clinical efficacy of transcutaneous electrical nerve stimulation (TENS) to relieve pain: a comprehensive review of factors influencing outcome. Medicina. 2021;57(4):378.
14. Carnicer-Lombarte A, Chen S-T, Malliaras GG, Barone DG. Foreign body reaction to implanted biomaterials and its impact in nerve neuroprosthetics. Front Bioeng Biotechnol, p. 271, 2021.
15. McConnell GC, Rees HD, Levey AI, Gutekunst C-A, Gross RE, Bellamkonda RV. Implanted neural electrodes cause chronic, local inflammation that is correlated with local neurodegeneration. J Neural Eng. 2009;6(5):056003.
16. Krauss JK, et al. Technology of deep brain stimulation: current status and future directions. Nat Reviews Neurol. 2021;17(2):75–87.
17. Rastogi P, Lee E, Hadimani RL, Jiles DC. Transcranial Magnetic Stimulation-Coil design with improved focality. AIP Adv, 7, 5, 2017.
18. Khokhar FA, Voss LJ, Steyn-Ross DA, Wilson MT. Design and demonstration in vitro of a mouse-specific transcranial magnetic stimulation coil. IEEE Trans Magn. 2021;57(7):1–11.
19. Gomez L, Koponen L, Hamdan R, Goetz S, Peterchev A. Practical TMS coils with maximum focality and various stimulation depths, *Brain Stimulation: Basic, Translational, and Clinical Research in Neuromodulation*, vol. 14, no. 6, p. 1695, 2021.
20. Gomez LJ, Goetz SM, Peterchev AV. Design of transcranial magnetic stimulation coils with optimal trade-off between depth, focality, and energy. J Neural Eng. 2018;15(4):046033.
21. Zhong G, Yang Z, Jiang T. Precise modulation strategies for transcranial magnetic stimulation: advances and future directions. Neurosci Bull pp. 1–17, 2021.
22. Mizutani-Tiebel Y, et al. Concurrent TMS-fMRI: technical challenges, developments, and overview of previous studies. Front Psychiatry. 2022;13:825205.
23. Arslan S, Ktena SI, Makropoulos A, Robinson EC, Rueckert D, Parisot S. Human brain mapping: a systematic comparison of parcellation methods for the human cerebral cortex. NeuroImage. 2018;170:5–30.
24. Han IK et al. Electroconductive, Adhesive, Non-Swelling, and Viscoelastic Hydrogels for Bioelectronics (Adv. Mater. 4/2023), *Advanced Materials*, vol. 35, no. 4, p. 2370028, 2023.
25. Wen X, et al. Flexible, multifunctional neural probe with liquid metal enabled, ultra-large tunable stiffness for deep-brain chemical sensing and agent delivery. Biosens Bioelectron. 2019;131:37–45.
26. Chen JC, et al. A wireless millimetric magnetoelectric implant for the endovascular stimulation of peripheral nerves. Nat Biomedical Eng. 2022;6(6):706–16.
27. Charthad J, et al. A mm-sized wireless implantable device for electrical stimulation of peripheral nerves. IEEE Trans Biomed Circuits Syst. 2018;12(2):257–70.
28. Chen P et al. Wireless Deep Brain Stimulation by Ultrasound-Responsive Molecular Piezoelectric Nanogenerators. ACS Nano, 2023.
29. Chen JC et al. Self-rectifying magnetoelectric metamaterials for remote neural stimulation and motor function restoration. Nat Mater, pp. 1–8, 2023.
30. Prodanov D, Delbeke J. Mechanical and biological interactions of implants with the brain and their impact on implant design. Front NeuroSci. 2016;10:11.
31. Koo J, et al. Wireless bioresorbable electronic system enables sustained nonpharmacological neuroregenerative therapy. Nat Med. 2018;24(12):1830–6.
32. Kozielski KL, et al. Nonresonant powering of injectable nanoelectrodes enables wireless deep brain stimulation in freely moving mice. Sci Adv. 2021;7(3):eabc4189.
33. Balanis CA. Advanced engineering electromagnetics. Wiley; 2012.
34. Sun X, Yuan B, Sheng L, Rao W, Liu J. Liquid metal enabled injectable biomedical technologies and applications. Appl Mater Today. 2020;20:100722.
35. Zhang Q et al. A laminated gravity-driven Liquid Metal-Doped Hydrogel of Unparalleled Toughness and Conductivity. Adv Funct Mater, p. 2308113, 2023.
36. Zhang J, Sheng L, Jin C, Liu J. Liquid metal as connecting or functional recovery channel for the transected sciatic nerve, *arXiv preprint arXiv:1404.5931*, 2014.
37. Tang R, et al. Towards an artificial peripheral nerve: Liquid metal-based fluidic cuff electrodes for long-term nerve stimulation and recording. Biosens Bioelectron. 2022;216:114600.
38. Duan M, et al. Phase-transitional Bismuth-Based metals enable Rapid Embolotherapy, Hyperthermia, and Biomedical Imaging. Adv Mater. 2022;34(42):2205002.
39. Wang X, et al. Printed conformable liquid metal e-skin-enabled spatiotemporally controlled bioelectromagnetics for wireless multisite tumor therapy. Adv Funct Mater. 2019;29(51):1907063.
40. Peterchev AV, Deng ZD, Goetz SM. Advances in transcranial magnetic stimulation technology. Brain Stimulation: Methodologies Interventions, pp. 165–89, 2015.
41. Zhang S, Yin T, Liu Z, Li Y, Jin J, Ma R. Experimental study to improve the focalization of a figure-eight coil of rTMS by using a highly conductive and highly permeable medium. IEEE Trans Neural Syst Rehabil Eng. 2012;21(3):364–9.
42. Stenroos M, Koponen L. Real-time computation of the TMS-induced electric field in a realistic head model. NeuroImage, 203, Article 116159, ed, 2019.
43. Wang Q, Yu Y, Pan K, Liu J. Liquid metal angiography for mega contrast X-ray visualization of vascular network in reconstructing in-vitro organ anatomy. IEEE Trans Biomed Eng. 2014;61(7):2161–6.
44. He Y, You J, Dickey MD, Wang X. Controllable flow and manipulation of liquid metals. Adv Funct Mater. 2024;34(31):2309614.
45. Yang N, et al. Injectable nonmagnetic liquid metal for Eddy-thermal ablation of tumors under alternating magnetic field. Small Methods. 2020;4(9):2000147.

46. Wang D et al. Non-magnetic injectable implant for magnetic field-driven thermochemotherapy and dual stimuli-responsive drug delivery: transformable liquid metal hybrid platform for cancer theranostics, *Small*, vol. 15, no. 16, p. 1900511, 2019.
47. Zhang Q, et al. A laminated gravity-driven liquid metal-doped hydrogel of unparalleled toughness and conductivity. Adv Funct Mater. 2024;34(31):2308113.
48. Lu Y, et al. Transformable liquid-metal nanomedicine. Nat Commun. 2015;6(1):10066.
49. Wang D, Wang X, Rao W. Precise regulation of Ga-based liquid metal oxidation. Acc Mater Res. 2021;2(11):1093–103.
50. Wu X et al. Self-Adaptive Magnetic Liquid Metal Microrobots Capable of Crossing Biological Barriers and Wireless Neuromodulation. ACS Nano, 2024.
51. Yang N, et al. Liquid metal microspheres with an eddy-thermal effect for magnetic hyperthermia-enhanced cancer embolization-immunotherapy. Sci Bull. 2023;68(16):1772–83.
52. Xiang W et al. Liquid-metal-based magnetic fluids. Nat Reviews Mater pp. 1–17, 2024.

## Publisher's note